2018 IEEE/RSJ International Conference on Intelligent Robots and Systems (IROS)
Madrid, Spain, October 1-5, 2018

Dual-arm Coordinated Motion Planning and Compliance Control for Capturing Moving Objects with Large Momentum

Lei Yan[1], Yiming Yang[2], Wenfu Xu[1*], and Sethu Vijayakumar[2]

***Abstract*— Capturing a moving object with large momentum by a dual-arm robot is especially challenging because of the requirement of dual-arm coordinated motion planning for tracking the moving object, and the operational force control for contact and momentum transfer. In this paper, we present a dual-arm coordinated motion planning and compliance control method with a unique null-space projected relative Jacobian and relative operational force between the two arms. The proposed method is able to plan dual-arm capturing motion and control the capturing force without disturbing the tracking motion. We have also adopted a direct collocation trajectory optimization method to generate optimal trajectory to decrease the object's momentum with minimum effort. Simulation and experiment of dual-arm robots picking up a moving box on a mobile platform are carried out to verify the proposed method.**

I. Introduction

Compared with single manipulators, dual-arm robots have much better flexibility and adaptability in accomplishing heavy payload handling and assembling tasks. Meanwhile, the closed-chain constraint between the object and the dual-arm system also introduces more difficulties in modeling, planning and control of the coordinated operation. Existing researches mainly focus on the dual-arm coordinated operation of static objects, or moving objects with negligible mass. However, finding feasible solutions for capturing large moving objects with non-negligible mass and velocity is a common problem that may arise in many practical scenarios, such as on an assembling line as shown in Fig. 1.

Solving such problems is non-trivial, where the robot needs to avoid colliding with the moving obstacles as well as the target. Furthermore, the contact forces must be controlled carefully when capturing a heavy and moving object, otherwise the target object or even the robot itself can be damaged. Thus, we propose to split the problem into three phases: 1) *pre-contact phase*, i.e., find a collision-free trajectory to a pre-capturing posture; 2) *contact phase*, i.e., form stable contact with the object from the pre-capturing posture; and 3) *post-contact phase*, i.e., stop the object with the minimum effort, in order to facilitate desired manipulation.

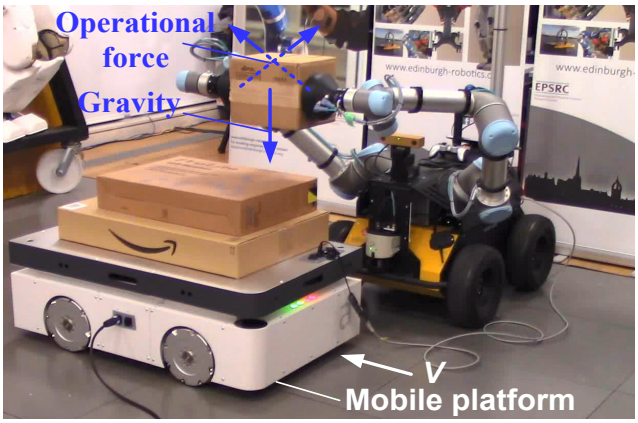

Fig. 1: Dual-arm robot capturing the moving target object.

The pre-contact phase can be seen as a classical motion planning problem, but in a changing environment. Motion planning is one of the fundamental problems in robotics, involving automatically finding a sequence of configurations that take the robot from a start to a goal pose. In the past two decades, sampling-based planning algorithms such as Rapidly-exploring Random Tree (RRT, [1]), Probabilistic Roadmap (PRM, [2]) and many others, have shown the ability of solving high-dimensional motion planning problems in complex environments. However, most of these algorithms are designed for static environments. Time-configuration space was proposed in [3] for avoiding moving obstacles using a unidirectional search algorithm. Approaches such as velocity obstacles [4] are commonly used for generating collision-free trajectories in the presence of moving obstacles, but normally do not scale to complex environments.

Salehian et al. [5] proposed a coordinated multi-arm motion planning method for reaching moving objects with motion uncertainty, which can generate autonomous and synchronized motions using the virtual object based dynamic system. A similar dynamic system is also used to catch a flying object softly [6]. However, the momentum transfer was bypassed by assuming the large object moves very slowly in [5] and the flying object has a negligible mass in [6]. The internal force analysis and load distribution for cooperative manipulation have been studied in [7], [8]. Korayem et al. [9] compared the dynamic load-carrying capacity of a multi-arm robot in the free mode and constrained mode by

This work was supported by the National Natural Science Foundation of China (Grant No. 61573116), the Basic Research Program of Shenzhen (CKFW2016033016372515) and China Scholarship Council. This work was also supported in part by the Engineering and Physical Sciences Research Council under Grant EP/R026173/1, EP/R026092/1 and UKIERI-DST 2016-17-0152.

[1]Lei Yan and Wenfu Xu are with the School of Mechanical Engineering and Automation, Harbin Institute of Technology, Shenzhen, 518055, China. (e-mail: lyan0825@gmail.com, wfxu@hit.edu.cn). Wenfu Xu is the corresponding author.

[2]Yiming Yang and Sethu Vijayakumar are with the Institute of Perception, Action and Behaviour, School of Informatics, University of Edinburgh, Edinburgh, EH8 9AB, U.K. (e-mail: yiming.yang@ed.ac.uk, sethu.vijayakumar@ed.ac.uk).

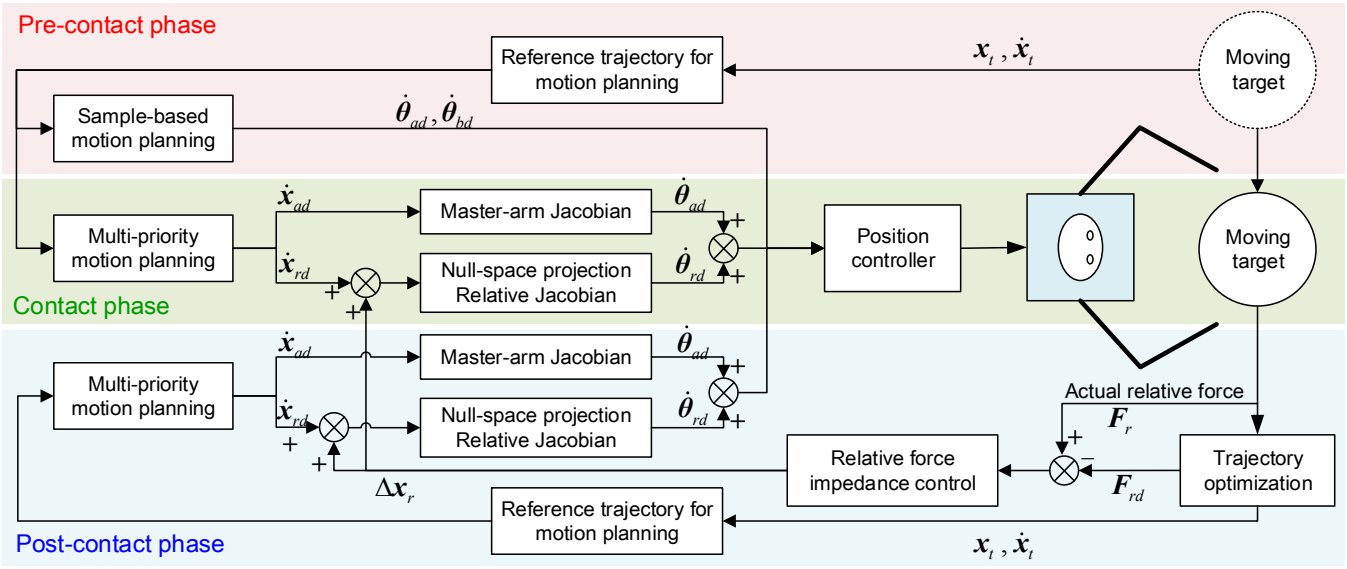

Fig. 2: Overview of the control pipeline for the capturing process. The whole process is decomposed into three phases: *pre-contact phase* (Section II), *contact phase* (Section III) and *post-contact* (Section IV). Note that the trajectory optimization is computed offline.

load distribution optimization, however, the solution for the dynamic closed-chain circumstance was not considered.

Many researches on multi-finger grasping can also be applied in multi-arm manipulation as they share certain similar concepts. Roa et al. [10] reviewed the grasp quality measures from the aspects of positions of contact points and hand configurations. Koval et al. [11] studied the pre-/post-contact policy decomposition for planar contact manipulation. Wimbck et al. [12], [13] proposed the object-level impedance controller for dynamic dexterous manipulation. However, one disadvantage is the fact that the springs should be designed in a compatible way. An adaptive compliant grasp control strategy was proposed in [14] for in-hand manipulation with position uncertainty. The compliance was also adopted in the master-slave and shared force control approaches for dual-arm coordinated operation [15]. However, there is little research that describes the unresolved issue of making contacts with the large moving objects.

In order to reduce the momentum of the moving object after contact, an optimal trajectory of the object should be provided to minimize the operational force for the robot's end-effectors. Recently, a purely kinematic trajectory optimization method was proposed to manipulate in-grasp object with relaxed-rigidity constraints [16]. Betts et al. [17] reviewed the numerical method for trajectory optimization, and discussed the direct and indirect methods. In this paper, we adopt the direct collocation method in [18] to generate an optimal trajectory for the post-contact phase of capturing a moving object.

To capture moving objects with large momentum, we decompose the whole task into the three phases and solve them sequentially. While the pre-contact and post-contact phases are solved by combining existing methods, this work proposes a novel algorithm for solving the second sub-task, i.e. coordinated compliance control during the contact phase, with the following contributions:

1) The dual-arm relative operational force is derived, which is compatible with the relative Jacobian;
2) A dual-arm coordinated compliance control method is proposed, where the master arm is used to track the object and the relative motion and force between two arms are controlled for capturing the object;
3) An overall framework for capturing moving objects with large momentum, enabling dual-arm robots for more general and complex tasks;

An overview of the control pipeline is highlighted in Fig. 2, where the three phases are described in Section II, III and IV respectively. In Section V, we verify the proposed method by the rigid multi-body dynamics simulation and hardware experiment in which a NASA's Valkyrie humanoid robot model and a real dual-arm Husky robot are used to capture a moving object on a mobile platform, followed by the conclusion in Section VI.

II. Pre-Contact Phase: Collision-Free Motion Planning in Changing Environments

In order to manipulate the target object, the robot needs to first move to a pre-contact posture. Such step is normally less important in simple and static environments where the robot can move freely without considering collision avoidance. However, as highlighted in Fig. 1, in scenarios where the robot is very close to collision objects in the environment, finding a collision-free trajectory to move to the pre-contact posture is non-trivial.

To address the collision-free motion planning problem in changing environments, we have adopted the *time-configuration* space sampling-based planner [19] and extended it to work with bi-manual systems. Consider an N Degree-of-Freedom (DoF) robot, let $\boldsymbol{\theta} \in \mathcal{C}$ be the joint state in the configuration space $\mathcal{C} \subset \mathbb{R}^N$. There should be safe distances between the two end-effectors and the target for further contacting and capturing. Given the desired

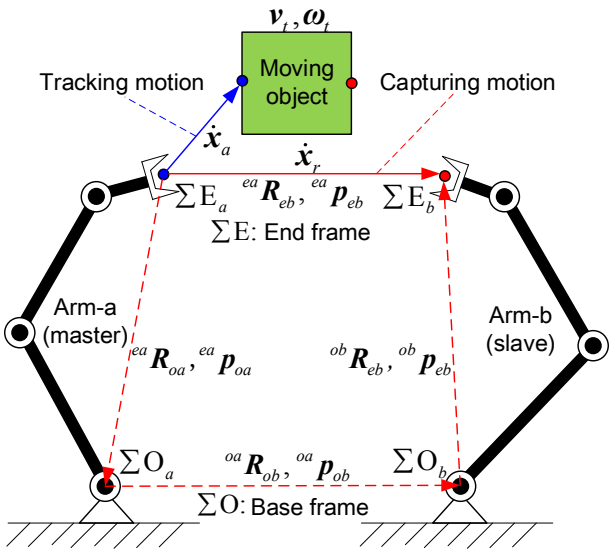

Fig. 3: Dual-arm coordinated motion during the capture process.

poses $\boldsymbol{x}_{ad}$ and $\boldsymbol{x}_{bd}$ of the two end-effectors according to the target's pose, the desired joint positions $\boldsymbol{\theta_d}$ can be calculated using inverse kinematics (IK). We assume that the collision environment is non-static but the change over time is known, i.e. $env(t)$ is given. A time-configuration space, $\mathcal{S} \subset \mathcal{C} \times \mathbb{R}$, is created, where an extra dimension has been appended to the configuration space which represents the time axis. Given start and goal states in the time-configuration space, $\mathbf{s}_0 = \langle \boldsymbol{\theta}_0, 0 \rangle$ and $\mathbf{s}_T = \langle \boldsymbol{\theta}_T, T \rangle$, the planning problem is defined as:

$$\begin{aligned} \boldsymbol{\theta}_{[0:T]} &= \text{PreContactPlanning}(\mathbf{s}_0, \mathbf{s}_T, env(t)) \\ s.t. \quad & \forall t \in [0, T] : CollisionFree(\boldsymbol{\theta}_t, env(t)) \end{aligned} \tag{1}$$

where $CollisionFree$ means the two arms won't collide with the environment or collide with each other.

After reaching the pre-contact posture, the two arms can be controlled by the following dual-arm coordinated compliance control for further manipulation.

III. Contact Phase: Dual-arm Coordinated Compliance Control

A. Multi-priority Motion Planning based on Relative Jacobian and Null-space Projection

In the situation of capturing a moving object, the relative position and orientation of two arms need to satisfy the coordinated constraint to capture the object while each arm should also track and reach the desired capturing points, making the planning and control for each manipulator very challenging.

Without loss of generality, assume the left arm "Arm-a" as the master arm which is used for tracking the capturing point, and the right arm "Arm-b" as the slave, as shown in Fig. 3. Dual-arm coordinated capturing motion is realized in the null space of Arm-a's motion using *relative Jacobian* [20], [21]. The relative Jacobian is especially suitable for the dual-arm coordination problems, in which one manipulator provides the pose reference and the other one performs the corresponding coordinated operation task.

Given the Jacobian matrices $\boldsymbol{J}_a(\boldsymbol{\theta}_a)$ and $\boldsymbol{J}_b(\boldsymbol{\theta}_b)$ of each manipulator, the relative Jacobian matrix $\boldsymbol{J}_r(\boldsymbol{\theta})$ is defined as

$$\boldsymbol{J}_r = [-{}^{ea}\boldsymbol{\psi}_{eb}\, {}^{ea}\boldsymbol{\Omega}_{oa}\boldsymbol{J}_a \quad {}^{ea}\boldsymbol{\Omega}_{ob}\boldsymbol{J}_b], \tag{2}$$

where ${}^{i}\boldsymbol{\psi}_j = \begin{bmatrix} \boldsymbol{I} & -({}^{i}\boldsymbol{p}_j)^{\times} \\ \boldsymbol{O} & \boldsymbol{I} \end{bmatrix}$, ${}^{i}\boldsymbol{\Omega}_j = \begin{bmatrix} {}^{i}\boldsymbol{R}_j & \boldsymbol{O} \\ \boldsymbol{O} & {}^{i}\boldsymbol{R}_j \end{bmatrix}$, ${}^{i}\boldsymbol{p}_j$ is the position vector from the origin of frame $\{i\}$ to the origin of frame $\{j\}$ with respect to frame $\{i\}$, $\{\boldsymbol{k}\}^{\times}$ is the skew symmetric matrix of $\boldsymbol{k}$, and ${}^{i}\boldsymbol{R}_j$ is the rotation matrix from frame $\{i\}$ to frame $\{j\}$.

Assuming the target's motion is known or predictable, then the desired end-effector motion $\dot{\boldsymbol{x}}_{ad}$ of the master arm for tracking and the desired relative motion $\dot{\boldsymbol{x}}_{rd}$ between two arms for capturing can be derived. Therefore, the joint angular velocity of the master arm can be obtained:

$$\dot{\boldsymbol{\theta}}_{ad} = \boldsymbol{J}_a^{\dagger}\dot{\boldsymbol{x}}_{ad}, \tag{3}$$

where $\boldsymbol{J}_a^{\dagger}$ represents the generalized inverse of $\boldsymbol{J}_a$.

In order not to disturb the master-arm's motion, dual-arm coordinated motion is planned in the null space of the master arm [22], which can be expressed as

$$\boldsymbol{N}_a = \boldsymbol{I} - \boldsymbol{J}_a^{\dagger}\boldsymbol{J}_a. \tag{4}$$

Thus, the relative Jacobian matrix $\boldsymbol{J}_r^{na}$ based on null-space projection can be expressed as

$$\boldsymbol{J}_r^{na} = \boldsymbol{J}_r\boldsymbol{N}_a = \boldsymbol{J}_r\left[\boldsymbol{I} - \boldsymbol{J}_a^{\dagger}\boldsymbol{J}_a\right]. \tag{5}$$

It is assumed that the desired relative velocity between the two arms represented in the end-effector frame of master arm is $\dot{\boldsymbol{x}}_{rd}$, then the desired angular velocity of each joint can be obtained according to (5) as

$$\dot{\boldsymbol{\theta}}_d = \begin{bmatrix} \dot{\boldsymbol{\theta}}_{ad} \\ \dot{\boldsymbol{\theta}}_{bd} \end{bmatrix} = \boldsymbol{J}_r^{na\dagger}\dot{\boldsymbol{x}}_{rd}. \tag{6}$$

The desired joint angular velocities of two arms for capturing the moving object can be obtained by adding (3) and (6). As the priority of the master arm's motion is higher than the dual-arm coordinated motion, the capturing motion would not affect the tracking motion. Thus, the control implementation is significantly simplified.

B. Dual-arm Coordinated Compliance Capturing Control

The objective of the contact process is to form stable contact and apply forces on the moving object by two arms to prevent dropping the object during the post-contact phase. In order to make contact with the moving object reliably, the motion sequence and operational force for two arms need to be planned simultaneously. While the dual-arm coordinated motion has been derived in Section III-A, the operational forces of two arms can be realized by impedance control. As shown in Fig. 4, the virtual spatial spring is established between two arms and the object. Traditionally, the compliance capturing control is realized by controlling the operational forces between each manipulator and the object separately. In our work, we simplify the control problem by presenting a relative operation force concept between the two arms (similar to the relative Jacobian). The proposed

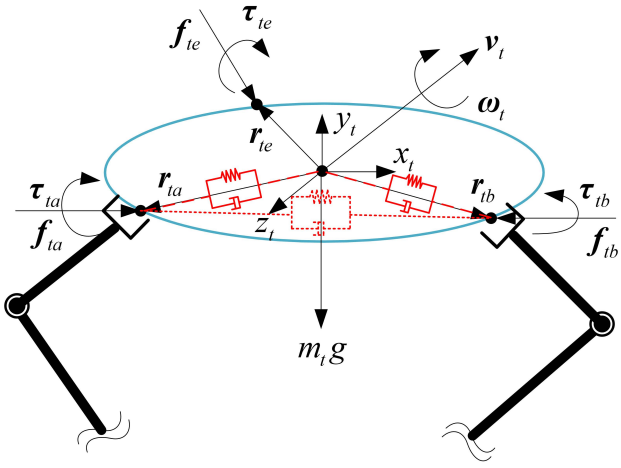

Fig. 4: Virtual spatial spring between two arms and the object.

method directly control the relative operational force which takes the operational forces of the two arms into account simultaneously.

In order to obtain the equivalent relative operational force $\boldsymbol{F}_r$ when performing dual-arm coordinated operation, it is necessary to represent the operational force $\boldsymbol{F}_{ea}$ and $\boldsymbol{F}_{eb}$ of the two arms with respect to one common reference coordinate system. In our work, the end-effector frame of the master arm is selected as the common reference coordinate system, therefore, the operational force of each arm can be rewritten as:

$$ {}^{r}\boldsymbol{F}_{ea} = [{}^{r}\boldsymbol{f}_{ea} \quad {}^{r}\boldsymbol{\tau}_{ea}] = {}^{ea}\boldsymbol{\Omega}_{oa}\boldsymbol{F}_{ea} \tag{7} $$

$$ {}^{r}\boldsymbol{F}_{eb} = [{}^{r}\boldsymbol{f}_{eb} \quad {}^{r}\boldsymbol{\tau}_{eb}] = {}^{ea}\boldsymbol{\Omega}_{ob}\boldsymbol{F}_{eb}. \tag{8} $$

where $\boldsymbol{f}$, $\boldsymbol{\tau}$ are the force and torque components of the operational force.

However, the operational force ${}^{r}\boldsymbol{F}_{ea}$ can also be treated as the effect of the operational force ${}^{r}\boldsymbol{F}'_{eb}$ (at the end-effector of Arm-b) on the end-effector of the master arm through the relative position vector ${}^{ea}\boldsymbol{p}_{eb}$,

$$ {}^{r}\boldsymbol{F}_{ea} = \begin{bmatrix} \boldsymbol{I} & \boldsymbol{O} \\ ({}^{ea}\boldsymbol{p}_{eb})^{\times} & \boldsymbol{I} \end{bmatrix} {}^{r}\boldsymbol{F}'_{eb} = {}^{ea}\boldsymbol{\psi}_{eb}^{T}\,{}^{r}\boldsymbol{F}'_{eb}. \tag{9} $$

Therefore, the relative operational force $\boldsymbol{F}_r$ can be obtained as

$$ \begin{aligned} \boldsymbol{F}_r &= {}^{r}\boldsymbol{F}_{eb} - {}^{r}\boldsymbol{F}'_{eb} = {}^{r}\boldsymbol{F}_{eb} - ({}^{ea}\boldsymbol{\psi}_{eb}^{T})^{-1}\,{}^{r}\boldsymbol{F}_{ea} \\ &= \begin{bmatrix} -({}^{ea}\boldsymbol{\psi}_{eb}^{T})^{-1\,ea}\boldsymbol{\Omega}_{oa} & {}^{ea}\boldsymbol{\Omega}_{ob} \end{bmatrix} \begin{bmatrix} \boldsymbol{F}_{ea} \\ \boldsymbol{F}_{eb} \end{bmatrix}. \end{aligned} \tag{10} $$

According to the principle of virtual work, the relationship between the relative operation force $\boldsymbol{F}_r$ and joint torque $\boldsymbol{\tau} = \begin{bmatrix} \boldsymbol{\tau}_a^T & \boldsymbol{\tau}_b^T \end{bmatrix}^T$ satisfies the following condition,

$$ \delta work = \boldsymbol{\tau}^T \delta\boldsymbol{\theta} - {\boldsymbol{F}_r}^T \delta\boldsymbol{x}_r = \left(\boldsymbol{\tau}^T - {\boldsymbol{F}_r}^T \boldsymbol{J}_r\right) \delta\boldsymbol{\theta} = 0 \tag{11} $$

yields,

$$ \boldsymbol{\tau} = {\boldsymbol{J}_r}^T \boldsymbol{F}_r, \tag{12} $$

Meanwhile, substituting (2) and (10) to (12), we can obtain

$$ {\boldsymbol{J}_r}^T \boldsymbol{F}_r = \begin{bmatrix} \boldsymbol{J}_a^T \boldsymbol{F}_{ea} \\ \boldsymbol{J}_b^T \boldsymbol{F}_{eb} \end{bmatrix} = \begin{bmatrix} \boldsymbol{\tau}_a \\ \boldsymbol{\tau}_b \end{bmatrix} = \boldsymbol{\tau}, \tag{13} $$

which shows that the relative operational force proposed in this paper is compatible with the relative Jacobian.

The relationship of the relative motion and relative force between the two arms is established by the "spring-damper-mass" mechanical system model. The position-based impedance control is realized by transforming the force deviation to the motion deviation as follows:

$$ \Delta\boldsymbol{x}_r = \frac{\Delta\boldsymbol{F}_r}{\boldsymbol{M}_d\boldsymbol{s}^2 + \boldsymbol{B}_d\boldsymbol{s} + \boldsymbol{K}_d} \tag{14} $$

where $\Delta\boldsymbol{x}_r = \boldsymbol{x}_r - \boldsymbol{x}_{rd}$, $\boldsymbol{x}_r$ and $\boldsymbol{x}_{rd}$ are the actual and desired relative motion between the two arms, respectively; $\Delta\boldsymbol{F}_r = \boldsymbol{F}_r - \boldsymbol{F}_{rd}$, $\boldsymbol{M}_d$, $\boldsymbol{B}_d$, and $\boldsymbol{K}_d$ are the ideal inertial, damping, and stiffness parameters for impedance control.

Finally, the dual-arm coordinated compliance control can be realized by directly adding $\Delta\boldsymbol{x}_r$ to $\dot{\boldsymbol{x}}_{rd}$ in (6).

$$ \dot{\boldsymbol{\theta}}_d = \boldsymbol{J}_r^{na\dagger} \left(\dot{\boldsymbol{x}}_{rd} + \Delta\boldsymbol{x}_r\right). \tag{15} $$

IV. Post-Contact Phase: Trajectory Optimization for Manipulating Objects with Large Momentum

After having stable contact with the object using the coordinated compliance control method proposed in Section III, the final phase is to manipulate the moving object to a desired pose with zero momentum. As shown in Fig. 4, the dynamic equation of the object during dual-arm coordinated operation can be written as

$$ \begin{aligned} &\begin{bmatrix} \boldsymbol{E} & \boldsymbol{O} \\ \boldsymbol{r}_{ta}^{\times} & \boldsymbol{E} \end{bmatrix} \begin{bmatrix} \boldsymbol{f}_{ta} \\ \boldsymbol{\tau}_{ta} \end{bmatrix} + \begin{bmatrix} \boldsymbol{E} & \boldsymbol{O} \\ \boldsymbol{r}_{tb}^{\times} & \boldsymbol{E} \end{bmatrix} \begin{bmatrix} \boldsymbol{f}_{tb} \\ \boldsymbol{\tau}_{tb} \end{bmatrix} + \begin{bmatrix} \boldsymbol{G}_t \\ \boldsymbol{O} \end{bmatrix} \\ &+ \begin{bmatrix} \boldsymbol{E} & \boldsymbol{O} \\ \boldsymbol{r}_{te}^{\times} & \boldsymbol{E} \end{bmatrix} \begin{bmatrix} \boldsymbol{f}_{te} \\ \boldsymbol{\tau}_{te} \end{bmatrix} = \begin{bmatrix} \boldsymbol{m}_t\dot{\boldsymbol{v}}_t \\ \boldsymbol{I}_t\dot{\boldsymbol{\omega}}_t + \boldsymbol{\omega}_t \times (\boldsymbol{I}_t\boldsymbol{\omega}_t) \end{bmatrix}, \end{aligned} \tag{16} $$

where $\boldsymbol{F}_{ta} = -\boldsymbol{F}_{ea} = [\boldsymbol{f}_{ta}, \boldsymbol{\tau}_{ta}]^T$ and $\boldsymbol{F}_{tb} = -\boldsymbol{F}_{eb} = [\boldsymbol{f}_{tb}, \boldsymbol{\tau}_{tb}]^T$ are the dual-arm operational forces exerted on the object; $\boldsymbol{F}_{te} = [\boldsymbol{f}_{te}, \boldsymbol{\tau}_{te}]^T$ is the external force exerted on the object; $\boldsymbol{r}_{ta}$ and $\boldsymbol{r}_{tb}$ are the vector from the centroid of the object to the contact points of the two arms, respectively; $\boldsymbol{v}_t$ and $\boldsymbol{\omega}_t$ are the linear and angular velocity of the object; and $\boldsymbol{m}_t$ and $\boldsymbol{I}_t$ are the mass and inertia matrix of the object.

In order to ensure that the system dynamics equation is in first-order form, the state vector of the system is written as

$$ \boldsymbol{s} = [\boldsymbol{x} \quad \dot{\boldsymbol{x}}]^T, \tag{17} $$

where $\boldsymbol{x} = [p_x, p_y, p_z, \alpha, \beta, \gamma]^T$ is the pose (position and orientation) of the object. The orientation of the object is represented by the Z-Y-X Euler angles.

For capturing the moving object, the non-negligible momentum should be decreased gradually without causing large operational forces at the robot's end-effectors. Therefore, the objective of the trajectory optimization is to manipulate the moving object to the desired pose with minimum operational forces, which can be formulated as

$$ \text{minimize:} \int_{t_0}^{t_f} \left(\sum \boldsymbol{F}_{ta}^2(i) + \sum \boldsymbol{F}_{tb}^2(i)\right) dt, \tag{18} $$

where the equation has the decision variables $\boldsymbol{x}(t)$, $\dot{\boldsymbol{x}}(t)$, $\boldsymbol{F}_{ta}(t)$, and $\boldsymbol{F}_{tb}(t)$, and is subject to the following constraints.

1) Boundary constraint: The boundary constraint is set to manipulate the object from the initial pose and velocity to the desired pose and velocity,

$$\boldsymbol{x}(t_0) = \boldsymbol{x}_0; \boldsymbol{x}(t_f) = \boldsymbol{x}_f; \dot{\boldsymbol{x}}(t_0) = \dot{\boldsymbol{x}}_0; \dot{\boldsymbol{x}}(t_f) = \dot{\boldsymbol{x}}_f. \quad (19)$$

In a general object manipulation scenario, the position and orientation of the object is changing continuously. As a consequence, the normal vectors of the contact surfaces will be also changing during the manipulation, which makes the contact constraint ill-defined. In order to simplify the expression of the end-effector constraint and the friction cone constraint, the operational forces are represented in the centroid frame of the object as ${}^t\boldsymbol{F}_{ta}$ and ${}^t\boldsymbol{F}_{tb}$. Then the normal and tangential vectors of the contact surfaces represented in the centroid frame of the object can be simplified to constant vectors.

2) End-effector constraint: Consider using two palm-type end-effectors that can form a compliance contact with the object only by pushing, the end-effector constraint can be formulated as

$${}^t\boldsymbol{F}_{ta} \cdot {}^t\boldsymbol{n}_a \geq 0; {}^t\boldsymbol{F}_{tb} \cdot {}^t\boldsymbol{n}_b \geq 0, \quad (20)$$

where ${}^t\boldsymbol{n}_a$ and ${}^t\boldsymbol{n}_b$ are the normal vectors of the contact surfaces of the two arms represented in the centroid frame of the object.

3) Friction constraint: The soft-finger contact friction model [23] is used for the contact modelling between the end-effectors and the object. In case of a soft-finger contact, the effects of torsion and shear forces combine and cannot be treated separately. Therefore, four components are considered: one normal force ${}^tF^i_{tx}$, two tangential forces ${}^tF^i_{ty}$, ${}^tF^i_{tz}$, and one torsional moment ${}^t\tau^i_{tx}$ around the normal vector of the contact surface. Therefore, the friction cone constraint is defined as

$$\frac{1}{\mu}\sqrt{{}^tF^{i\ 2}_{ty} + {}^tF^{i\ 2}_{tz}} + \frac{1}{\mu'}{}^t\tau^i_{tx} \leq {}^tF^i_{tx}, \quad (21)$$

where μ and μ' are the corresponding friction coefficient. Note that based on the soft-finger contact friction model, the independent controlled variables are three translational directions, and only one rotational direction along the normal vector of the contact surface.

4) Force limit constraint: Additionally, we apply operational force limit constraint to satisfy joint torque limit and ensure safety, which can be formulated as

$$\boldsymbol{F}^a_{min} \leq \boldsymbol{F}_{ta}(t) \leq \boldsymbol{F}^a_{max}; \ \boldsymbol{F}^b_{min} \leq \boldsymbol{F}_{tb}(t) \leq \boldsymbol{F}^b_{max}. \quad (22)$$

5) State limit constraint: Finally, to ensure the object is within the manipulatable workspace and ability of two arms, the state boundary during the whole trajectory is given as

$$\boldsymbol{x}_{min} \leq \boldsymbol{x}(t) \leq \boldsymbol{x}_{max}; \ \dot{\boldsymbol{x}}_{min} \leq \dot{\boldsymbol{x}}(t) \leq \dot{\boldsymbol{x}}_{max}. \quad (23)$$

Under the assumption that the contact points will not change during the whole manipulation, we can have the desired motion of the two arms from the optimal trajectory of the object. The initial value of the optimization results are set to be the final value at the end of the contact phase, therefore the desired operational forces during the whole contact phase can be obtained by fifth order polynomial interpolation of the initial and final operational forces.

TABLE I: Constraints for trajectory optimization.

Description	Variables	Values
Time scope	t	$\{0, 5\}$
Bound constraint	$\boldsymbol{x}_0$	$\{0, 0, 0, 0, 0, 0\}$
	$\dot{\boldsymbol{x}}_0$	$\{0.04, 0, 0, 0, 0, 0\}$
	$\boldsymbol{x}_f$	$\{0, 0, 0.2, 0, 0, 0\}$
	$\dot{\boldsymbol{x}}_f$	$\{0, 0, 0, 0, 0, 0\}$
State limit	$\boldsymbol{x}_{min}$	$\{0, 0, 0, -\pi, -\pi, -\pi\}$
	$\dot{\boldsymbol{x}}_{min}$	$\{-\infty, ..., -\infty\}$
	$\boldsymbol{x}_{max}$	$\{0.6, 0.6, 0.6, \pi, \pi, \pi\}$
	$\dot{\boldsymbol{x}}_{max}$	$\{\infty, ..., \infty\}$
Control limit	$\boldsymbol{u}_{min}$	$\{-80, ..., -80\}$
	$\boldsymbol{u}_{max}$	$\{80, ..., 80\}$

V. Evaluation

In order to verify the proposed method, we have conducted a simulation study with a NASA's Valkyrie humanoid robot. The time-configuration space RRT-Connect algorithm from EXOTica [19] is used to generate the collision-free pre-contact trajectory. For contact and post-contact phases, the proposed algorithm is verified by a co-simulation of MATLAB and ADAMS to analyze the dynamic interaction between the dual-arm system and the target. Additionally, the hardware experiment is also carried out with a dual-arm Husky robot.

A. Comparison with the naive method

We have setup a testing scenario where a 5 kg target object placed on a mobile platform that is moving at a constant velocity 0.04 m/s. The objectives are to track and capture the moving target, and move it to a 200 mm height above the mobile platform. The dual-arm robot is controlled by the proposed dual-arm coordinated compliance control method, and the desired trajectory of the target after contact is generated by the trajectory optimization method with the constraints highlighted in Table I. In contrast to the trajectory optimization, we have also implemented another naive method for the post-contact phase. In the naive method, the target trajectory is obtained by interpolating the initial pose and the desired pose directly, which is a common approach in many industrial applications.

The simulation result of the capturing process is shown in Fig. 5. For the pre-contact phase, i.e., 0s to 10s, it can be seen that the two arms can reach the desired pre-contact points near the target at desired time 10s without colliding with other moving objects and the mobile platform. In this paper, it is assumed that there won't be any collision during the contact and post-contact phases.

For the contact phase from 10s to 15s, the two arms are controlled to reach the contact points with the same velocity as the object while the relative force is controlled to be the same as the initial value of the trajectory optimization results. The desired and actual relative force in the capturing

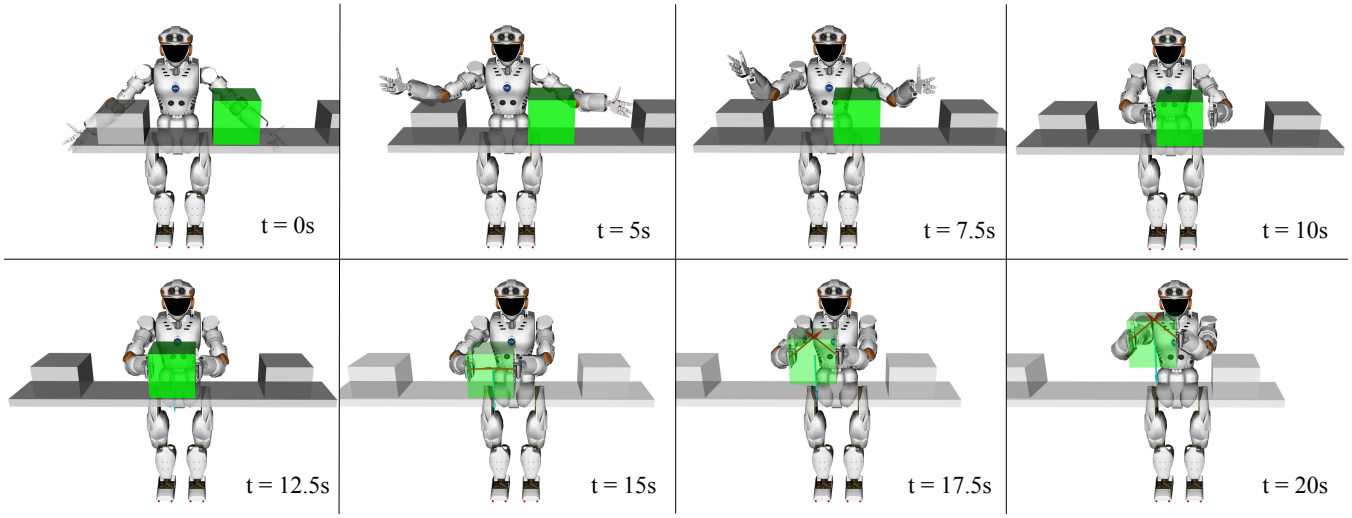

Fig. 5: The simulation results of capturing a moving object with the NASA Valkyrie robot.

direction during the simulation is shown in Fig. 6b. The plot shows that the dual-arm coordinated compliance control has a good performance in force tracking. Note that there exists some oscillations at the beginning of the contact phase at 12.5s. The relative force can be soon controlled to track the desired values after 13.2s.

Finally, for the post-contact phase from 15s to 20s, the dual-arm robot moves the object along a desired trajectory generated from the trajectory optimization. The master arm is used for tracking the object's optimal trajectory, while the relative motion and force between the two arms are controlled to manipulate the object without dropping it. The simulation results are shown in Fig. 6a and Fig. 6b. The maximum tracking error is 2.48 mm which is considerably small with respect to the desired value 200 mm, which is caused by the input trajectory and operational force error introduced by the interpolation.

The simulation result of the naive method is also shown in Fig. 6a and Fig. 6b, which is represented by "no optimization". In the naive method, the object's trajectory is obtained by interpolating the initial position $(0, 0, 0)$ and the final position $(0, 0, 200\text{mm})$ directly. There is a large operational force between the contact phase and post-contact phase at 15s, because the object's momentum was not taken into account and the trajectory was discontinuous. The maximum operational force is 144N, which is more than twice the desired value 65N. However, if the object follows the optimal trajectory obtained from the trajectory optimization, there will not be any trajectory discontinuity and large operational force between contact phase and post-contact phase.

B. Simulation with different mass, velocity and constraints

To further evaluate the proposed method, the same testing scenario is extended to include objects with different mass and velocity, i.e., (5kg, 0.04m/s), (10kg, 0.04m/s), and (10kg, 0.1m/s). The optimal trajectory and the optimal relative operational force are shown in Fig. 7a and Fig. 7b, respectively.

We have noticed that a significant amount of the forces has been used to compensate the object's gravity. Therefore, it is difficult to distinguish the difference between the optimal operational forces under different conditions. In order to show the effect of the workspace and operational force limits on the optimization result, we consider another set of simulation experiments where a 20kg object is moving at 1m/s in a gravity-free environment. Seven scenarios with different maximum operational force limit and state constraints for each axis are considered, i.e., (10N, 1m), (11N, 1m), (15N, 1m), (20N, 1m), (30N, 1m), (30N, 0.6m), and (30N, 0.4m). The optimization results in Fig. 8a and Fig. 8b show that, under force limits 15N and 20N, the algorithm generates different but valid trajectory and operational force. However, when the force limit is set to 10N, there does not exist any feasible solution. If we increase the force limit to 30N, the optimization result is identical to that with 20N force limit, i.e., the green and purple lines in Fig. 8, as the maximum required operational force during the process is only 16.66N. The same optimization results will be obtained when the force limit is higher than the required maximum force for the task.

Additionally, we have also compared the result of using the same 30N force limit but with different state limits, i.e., 1m, 0.6m and 0.4m. When the state limit is lower, a greater force will be generated in order to capture the object within the state limit and move it to the desired pose. Note that no valid solution exists if we further reduce the state limit to 0.4m, as the optimization is also subject to the force limit. From a gravity-free point of view, this method can be also used for space or on-orbit manipulation.

C. Experimental study

To further demonstrate the performance of the proposed method, hardware experiment has been carried out on a dual-arm Husky robot as shown in Fig. 9. The dual-arm Husky robot consists of a mobile base and two 6-DoF UR5 arms both fitted with the Robotiq FT 300 force/torque sensor. In our experiment, the robot base is fixed while two UR5 arms are controlled to capture the target object placed on another mobile platform. The initial conditions of the object

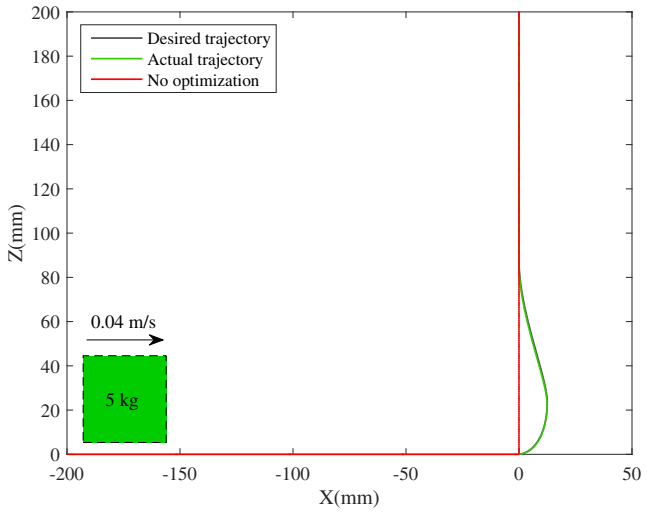

(a) The object trajectory during the manipulation.

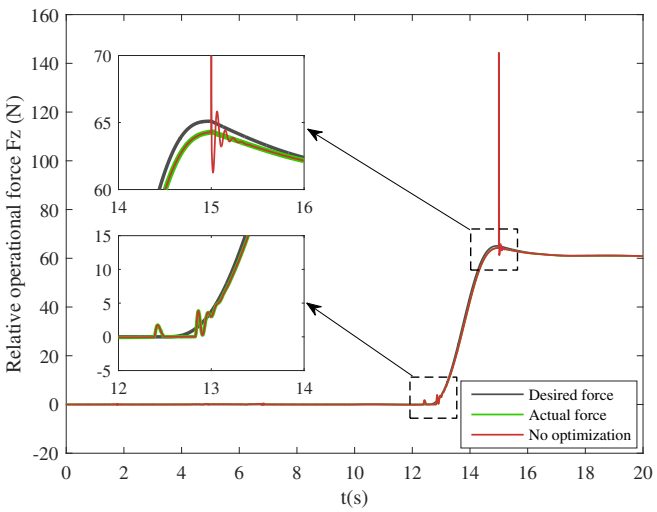

(b) The relative operational force during the manipulation.

Fig. 6: The object trajectory and the relative operational force, with the object mass set to 5 kg and the velocity set to 0.04 m/s.

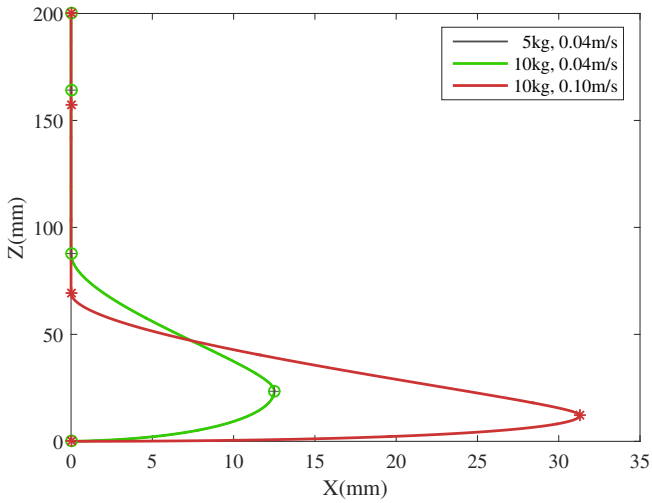

(a) The optimal trajectory with different mass and velocity.

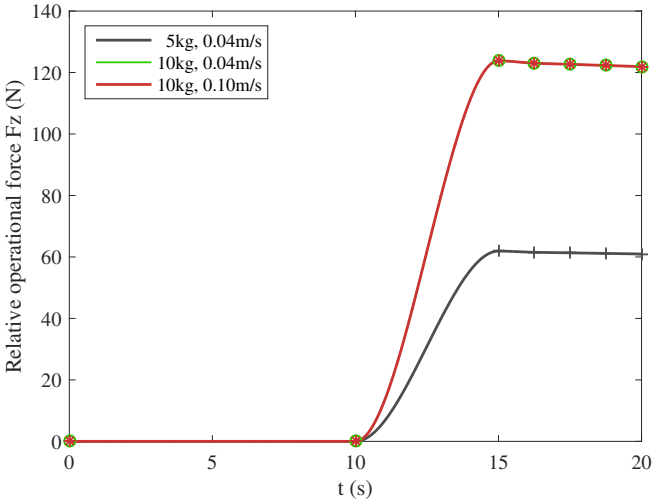

(b) The optimal force with different mass and velocity.

Fig. 7: The object trajectory and the relative operational force during the manipulation, with the different object mass and velocity.

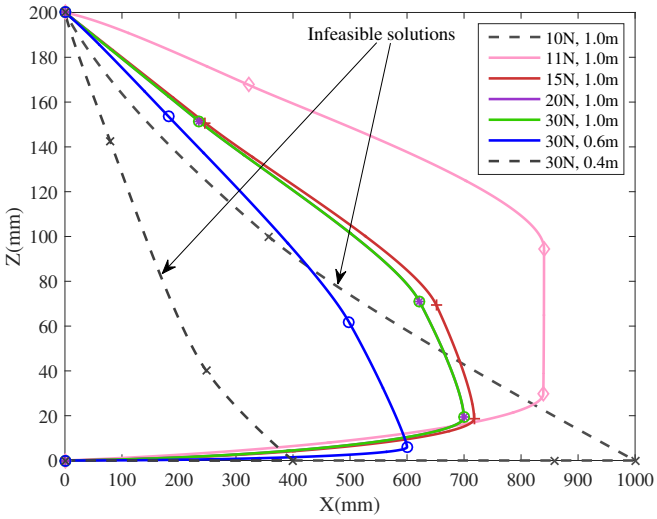

(a) The optimal trajectory with force and state limits.

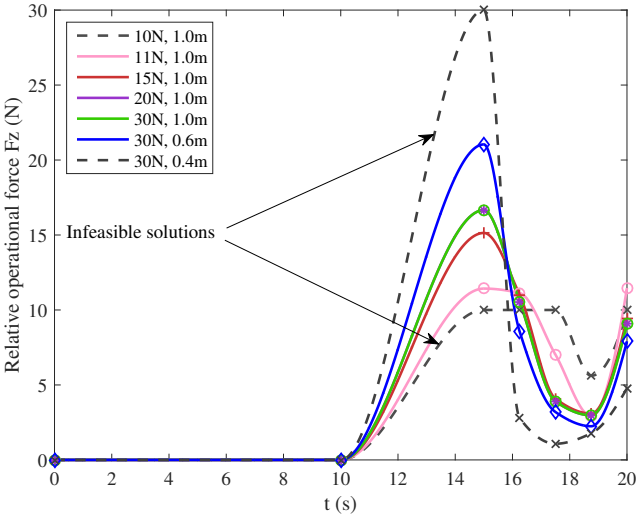

(b) The optimal force with force and state limits.

Fig. 8: The object trajectory and the relative operational force during the manipulation, with different operational force and state limits.

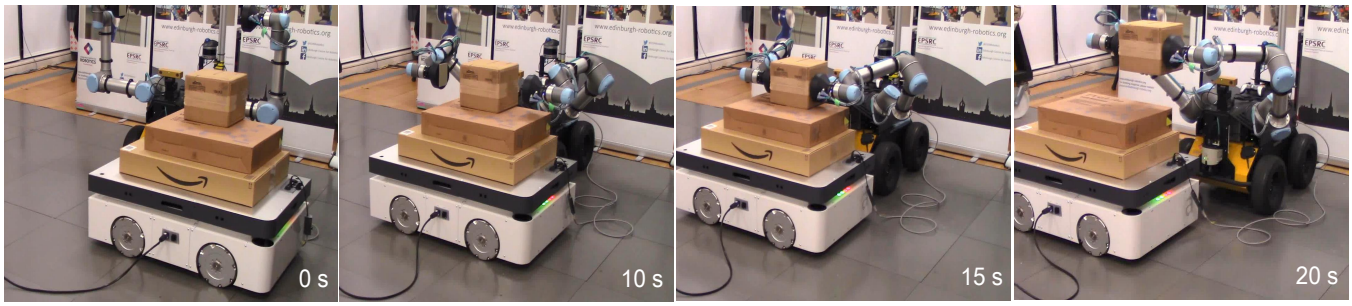

Fig. 9: Capturing a moving box with the dual-arm Husky robot.

are set to be the same as the simulation in Section V-A. All the planning and control algorithms are running in the on-board computer, and the control period is set to 10 ms. The experiment results show that the proposed method can successfully capture the moving target with non-negligible momentum, which also provides a feasible solution for the potential industrial applications.

VI. Conclusion

In this paper, we proposed a dual-arm coordinated motion planning and compliance control method for capturing moving object with non-negligible momentum. The method pipeline consists of three phases: 1) *pre-contact phase* where collision-free trajectories are generated using a time-configuration space sample-based planner to reach to a pre-contact posture; 2) *contact phase* where a dual-arm compliance control scheme is proposed, in which the master arm is used to track the object's motion while the relative motion and force between the two arms are controlled to catch the object; and 3) *post-contact phase* where a trajectory optimization is adopted to decrease the momentum gradually without causing large impact. Simulation and experiment results show that the proposed method can capture heavy and moving objects to a desired pose with desired force and minimum effort. Future work will include workspace and joint torque limits into the trajectory optimization by introducing the dynamics equation of the dual-arm robot.

References

[1] J. J. Kuffner and S. M. LaValle, "Rrt-connect: An efficient approach to single-query path planning," in *IEEE International Conference on Robotics and Automation (ICRA)*, 2000, pp. 995–1001.

[2] L. E. Kavraki, P. Svestka, J.-C. Latombe, and M. H. Overmars, "Probabilistic roadmaps for path planning in high-dimensional configuration spaces," *IEEE Transactions on Robotics and Automation*, vol. 12, no. 4, pp. 566–580, 1996.

[3] M. Cefalo, G. Oriolo, and M. Vendittelli, "Task-constrained motion planning with moving obstacles," in *IEEE/RSJ International Conference on Intelligent Robots and Systems (IROS)*, 2013, pp. 5758–5763.

[4] P. Fiorini and Z. Shiller, "Motion planning in dynamic environments using velocity obstacles," *The International Journal of Robotics Research*, vol. 17, no. 7, pp. 760–772, 1998.

[5] S. Sina Mirrazavi Salehian, N. Figueroa, and A. Billard, "Coordinated multi-arm motion planning: Reaching for moving objects in the face of uncertainty," in *Robotics: Science and Systems (RSS)*, 2016.

[6] S. S. M. Salehian, M. Khoramshahi, and A. Billard, "A dynamical system approach for softly catching a flying object: Theory and experiment," *IEEE Transactions on Robotics*, vol. 32, no. 2, pp. 462–471, 2016.

[7] S. Erhart and S. Hirche, "Internal force analysis and load distribution for cooperative multi-robot manipulation," *IEEE Transactions on Robotics*, vol. 31, no. 5, pp. 1238–1243, 2015.

[8] A. Z. Bais, S. Erhart, L. Zaccarian, and S. Hirche, "Dynamic load distribution in cooperative manipulation tasks," in *IEEE/RSJ International Conference on Intelligent Robots and Systems (IROS)*, 2015, pp. 2380–2385.

[9] M. Korayem, S. R. Nekoo, and R. A. Esfeden, "Dynamic load-carrying capacity of multi-arm cooperating wheeled mobile robots via optimal load distribution method," *Arabian Journal for Science and Engineering*, vol. 39, no. 8, pp. 6421–6433, 2014.

[10] M. A. Roa and R. Suárez, "Grasp quality measures: review and performance," *Autonomous Robots*, vol. 38, no. 1, pp. 65–88, 2015.

[11] M. C. Koval, N. S. Pollard, and S. S. Srinivasa, "Pre-and post-contact policy decomposition for planar contact manipulation under uncertainty," *The International Journal of Robotics Research*, vol. 35, no. 1-3, pp. 244–264, 2016.

[12] T. Wimbock, C. Ott, and G. Hirzinger, "Impedance behaviors for two-handed manipulation: Design and experiments," in *IEEE International Conference on Robotics and Automation (ICRA)*, 2007, pp. 4182–4189.

[13] T. Wimböck, C. Ott, A. Albu-Schäffer, and G. Hirzinger, "Comparison of object-level grasp controllers for dynamic dexterous manipulation," *The International Journal of Robotics Research*, vol. 31, no. 1, pp. 3–23, 2012.

[14] Z. Chen, T. Wimböck, M. A. Roa, B. Pleintinger, M. Neves, C. Ott, C. Borst, and N. Y. Lii, "An adaptive compliant multi-finger approach-to-grasp strategy for objects with position uncertainties," in *IEEE International Conference on Robotics and Automation (ICRA)*, 2015, pp. 4911–4918.

[15] L. Yan, Z. Mu, W. Xu, and B. Yang, "Coordinated compliance control of dual-arm robot for payload manipulation: Master-slave and shared force control," in *IEEE/RSJ International Conference on Intelligent Robots and Systems (IROS)*, 2016, pp. 2697–2702.

[16] B. Sundaralingam and T. Hermans, "Relaxed-rigidity constraints: In-grasp manipulation using purely kinematic trajectory optimization," in *Robotics: Science and Systems (RSS)*, 2017.

[17] J. T. Betts, "Survey of numerical methods for trajectory optimization," *Journal of Guidance, Control, and Dynamics*, vol. 21, no. 2, pp. 193–207, 1998.

[18] M. Kelly, "An introduction to trajectory optimization: How to do your own direct collocation," *SIAM Review*, vol. 59, no. 4, pp. 849–904, 2017.

[19] V. Ivan, Y. Yang, W. Merkt, M. P. Camilleri, and S. Vijayakumar, "Exotica: An extensible optimization toolset for prototyping and benchmarking motion planning and control," in *Robot Operating System (ROS)*. Springer, 2019, pp. 211–240.

[20] R. S. Jamisola and R. G. Roberts, "A more compact expression of relative jacobian based on individual manipulator jacobians," *Robotics and Autonomous Systems*, vol. 63, pp. 158–164, 2015.

[21] J. Lee, P. H. Chang, and R. S. Jamisola, "Relative impedance control for dual-arm robots performing asymmetric bimanual tasks," *IEEE Transactions on Industrial Electronics*, vol. 61, no. 7, pp. 3786–3796, 2014.

[22] A. Dietrich, C. Ott, and A. Albu-Schäffer, "An overview of null space projections for redundant, torque-controlled robots," *The International Journal of Robotics Research*, vol. 34, no. 11, pp. 1385–1400, 2015.

[23] M. Buss, H. Hashimoto, and J. B. Moore, "Dextrous hand grasping force optimization," *IEEE Transactions on Robotics and Automation*, vol. 12, no. 3, pp. 406–418, 1996.